In Vivo Viscoelasticity Estimation of Myocardium

Hiroshi Kanai
Department of Electronic Engineering, Graduate School of Engineering, Tohoku University,
Sendai 980-8579, Japan. Email: hkanai@ecei.tohoku.ac.jp

***Abstract*— Though myocardial viscoelasticity is essential in the evaluation of heart diastolic properties, it has never been non-invasively measured *in vivo*. By the ultrasonic measurement of the myocardial motion, we have already found that some pulsive waves are spontaneously excited by aortic-valve closure (AVC) at end-systole (T_0). In this study, a sparse sector scan at a sufficiently high frame rate clearly reveals *wave propagation* along the heart wall. The propagation time of the wave along the heart wall is very small, namely, *several milliseconds*, and cannot be measured by conventional equipment. From the measured phase velocity, we estimate the myocardial viscoelasticity *in vivo*. In *in vivo* experiments applied to 6 healthy subjects, 3 patients with hypertrophic cardiomyopathy (HCM), and 3 patients with aortic stenosis (AS), the propagation of the pulsive wave was clearly visible in all subjects. For the frequency component up to 90 Hz, the typical propagation speed is about several m/s and rapidly decreased around the time of AVC. For the healthy subject, the typical value of elasticity was about 24-30 kPa and did not change around the time of AVC. The typical transient values of viscosity decreased rapidly from 400 Pa·s to 70 Pa·s around the time of AVC. The measured shear elasticity and viscosity in this study are comparable to those obtained for the human tissues using audio frequency in *in vitro* experiments reported in the literature. The method cannot be easily applied to these patients because there were inhomogeneities in the phase velocities due to the diseased myocardium. By applying the measurement of the phase velocity to each of 5 layers set in the heart wall, the phase velocity in the middle layer was lower than those in the LV- and RV-sides of the heart wall, which will corresponds to the change in myocardial fiber orientations. This method offers potential for *in vivo* imaging of the spatial distribution of the passive mechanical properties of the myocardium, which cannot be obtained by conventional echocardiography, CT, or MRI.**

I. Introduction

Conventional ultrasonography, computer tomography (CT), and magnetic resonant imaging (MRI) enable clinical visualization of cross-sectional images of the human heart, but their imaging is restricted to large motion ($>$ 1 mm) and low frequency components ($<$ 30 Hz). The tissue Doppler imaging (TDI) technique enables determination of motion distribution of the myocardium in real time. Even in current measurement, however, the sampling frequency of the motion of the heart wall is low (at most 200 Hz [1]), that is, the sampling period is 5 ms, which is too long to detect the propagation time of the wave.

To measure the original vibrations of the heart sounds, we have already developed a method to transcutaneously measure the heart-wall vibrations as a waveform at one point or multiple points preset along an ultrasonic beam in the heart wall [2]. We found that there is a steep dip in the pulse which occurs exactly at the time of AVC (T_0) [3] as shown in **Fig. 1**. This *notch* has been also measured by the TDI approach to determine the time of AVC (T_0).

As shown in the upper figure of **Fig. 1**, use of the sparse sector scan [3] has allowed us to simultaneously measure heart-wall motion at 160 points at a sufficiently high frame rate to measure the propagation of the *notch pulse* along the interventricular septum (IVS). From consecutively obtained spatial distributions of the phase value of the vibration wave, our study [4] has revealed for the first time that the steep dip of the notch pulse propagates along the IVS from the base to the apex, and its phase velocity is determined. By analyzing various frequency components up to 90 Hz, the propagation speed shows the frequency dispersion.

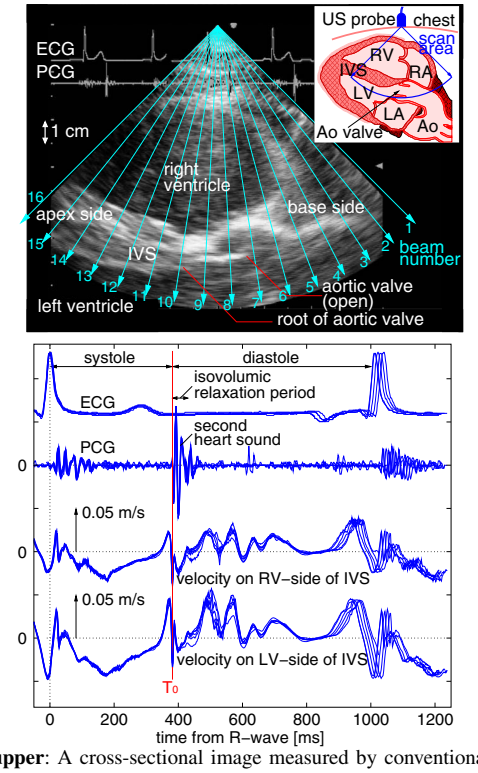

Fig. 1. **upper**: A cross-sectional image measured by conventional echocardiography in a healthy young male (subject A). The upper-right illustration shows the scanning range of the ultrasonic beams in this imaging. The arrows show the directions of the 16 ultrasonic beams used to measure the vibrations at about 160 points in the heart wall. **lower**: *In vivo* measurement results for the healthy man at two points set along the 13th ultrasonic beam. Each waveform for six consecutive cardiac cycles is overlaid.

This study shows that this dispersion characteristic agrees with the theoretical one of the Lamb wave which propagates in the *viscoelastic plate immersed in fluid*. By introducing the

single Voigt model into the equation of the Lamb wave and fitting the derived theoretical phase velocity to the measured dispersion, the myocardial viscoelastic properties are determined noninvasively for the first time.

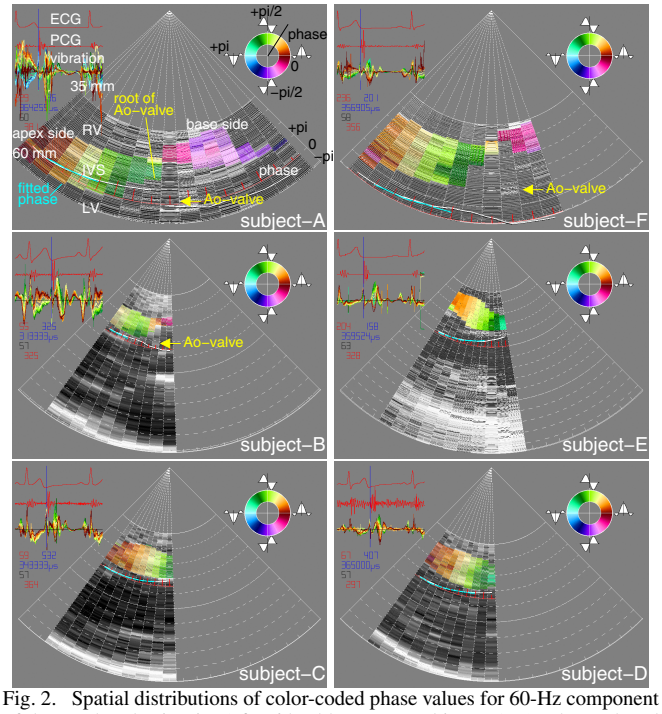

Fig. 2. Spatial distributions of color-coded phase values for 60-Hz component of the notch pulse in Fig. 1 for 6 healthy young subjects (A-F). The analyzed time corresponds to AVC (T_0).

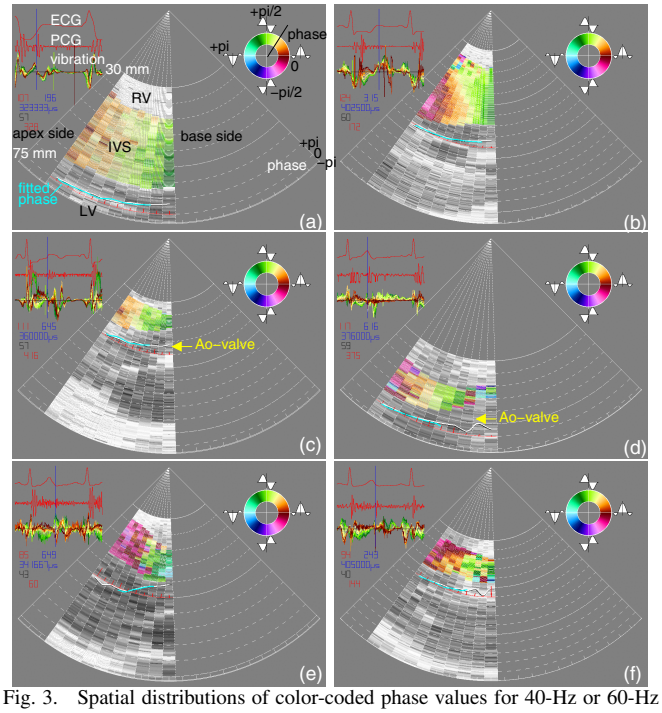

Fig. 3. Spatial distributions of color-coded phase values for 40-Hz or 60-Hz components of the notch pulse in Fig. 1 for 3 patients with HCM (a)-(c), and 3 patients with AS (d)-(f). The analyzed time corresponds to AVC (T_0).

II. Propagation of Pulsive Wave Along Heart Wall

Using a sparse sector scan in 16 directions, multiple points were preset at 770-μm intervals in the heart wall along each of 16 ultrasonic beams, and the vibrations at about 160 points were simultaneously measured as waveforms with a sampling frequency of 450 Hz by the phased tracking method [3].

Since the wavelength of the detected pulsive wave is about 100 mm for a 30-Hz component and is comparable to the size of the whole heart, its propagation phenomenon cannot be clearly visualized by showing the spatial distribution of the instantaneous *amplitude* of the pulsive wave. Therefore, using the method in [3], 2-D spatial distribution of the instantaneous *phase* values of the measured wave is shown in **Fig. 2**. For this imaging, the short-time Fourier transform is applied to the pulsive wave at each point in **Fig. 1** after the pulsive wave is multiplied by the Hanning window with a short length of 35 ms. The phase value is detected for each frequency component from 10 Hz to 90 Hz, and then color-coded based on the upper-right circular figure. **Figure 2** shows the phase distributions for a 60-Hz component along the IVS at a time of AVC (T_0) for 6 healthy young subjects. For 3 patients with HCM, and 3 patients with AS, the results are shown in **Fig. 3**.

From the consecutively obtained cross-sectional 2-D images, a motion picture is presented. It can be seen that a few pulsive waves are radiated from the root of aortic valve and propagate along the IVS. The delay due to the propagation of the pulse from the root to the apex is several milliseconds, which has not been recognized at all by any other clinical technique.

III. Estimation of Viscoelasticity Using Lamb Wave and Voigt Models

To determine the instantaneous phase velocity of the pulsive wave, if the straight line with a constant gradient k [rad/m] is spatially fit to the instantaneous spatial distribution of the measured phase in each cross-sectional image in **Fig. 2**, the instantaneous phase velocity for the frequency component f_0 is determined by $2\pi f_0/k$. However, since there is initially some spatial distribution of the phase which is independent of the propagation, the wavelength and thus the wave number k do not correspond to the actual phase velocity.

Therefore, in this study, based on the definition of the phase velocity, the distance Δx between two consecutively obtained phase distributions is determined. For this, the phase distribution $\theta(x;t)$ at a time t is compared with the shifted phase distribution $\theta(x+\Delta x; t-\Delta T)$ obtained at a time $t-\Delta T$.

Regarding the phenomenon of the wave propagation along the viscoelastic plate with thickness $2h$, there are three kinds of plate wave. In the parasternal longitudinal-axis view, the direction $(-y)$ of each ultrasonic beam is almost perpendicular to the IVS, and the detected motion is along each beam (y-direction in **Fig. 4**). The pulsive wave propagates along the IVS (x-direction). The vibrations at the RV-side and those at the LV-side are almost parallel (asymmetric). The wavelength λ is about 100 mm for the 30-Hz component and $40-65$ mm for the 90-Hz component. The thickness $2h$ of the IVS is about 10

mm in healthy adults. Thus, the thickness is sufficiently thin. The separate *in vivo* experiments show that the longitudinal component with x-displacement also propagates along the IVS (x-direction). The propagation speed of the shear component is seen to be close to that of the longitudinal component. Thus, there is a likelihood of coupling between the SV-component and the longitudinal component. Given these facts, the detected vibration signal can be modeled by a *Lamb wave with asymmetric mode* in **Fig. 4**.

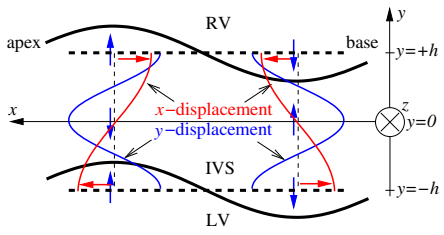

Fig. 4. Lamb wave with asymmetric mode of plate waves in the viscoelastic plate with thickness $2h$. The SV-wave component (y-displacement) and longitudinal component (x-displacement) are coupled, and the Lamb wave then propagates along the x-direction.

For the IVS, the blood in RV and LV should be considered. Thus, the model of *the Lamb wave propagating along the viscoelastic plate immersed in blood*, is employed in the present study. Let us define the wave number of the Lamb wave by $k_{\rm L}$. By referring to [5, Eq. (4.24)], the function, termed $f(k_{\rm L}, k_{\rm p}, k_{\rm s})$, which should be zero, is given by

$$\begin{aligned} f(k_{\rm L}, k_{\rm p}, k_{\rm s}) \;=\; & 4k_{\rm L}^2\eta\beta\cosh(\eta h)\sinh(\beta h) \\ & -(2k_{\rm L}^2 - k_{\rm s}^2)^2\sinh(\eta h)\cosh(\beta h) \\ & -\frac{\rho_{\rm b}\eta k_{\rm s}^4}{\rho_{\rm m}\eta_{\rm b}}\cosh(\eta h)\cosh(\beta h) = 0, \quad (1) \end{aligned}$$

where $k_{\rm p}$ and $k_{\rm s}$ are the wave numbers of the primary wave and the secondary wave, respectively. Using the wave number $k_{\rm b}$ in blood, η=$\sqrt{k_{\rm L}^2 - k_{\rm p}^2}$, β=$\sqrt{k_{\rm L}^2 - k_{\rm s}^2}$, and $\eta_{\rm b}$=$\sqrt{k_{\rm L}^2 - k_{\rm b}^2}$. $\rho_{\rm m}$ and $\rho_{\rm b}$ are the myocardium density and the blood density, respectively, and $\rho_{\rm m}$ can be approximated by $\rho_{\rm b}$=1.1×10^3 kg/m^3. The thickness $2h$ of the IVS is determined from the B-mode image.

By introducing a single Voigt dash-pot model in the frequency range up to 90 Hz, the Lamé elastic constants λ and μ become complex values as λ=λ_1+j$\omega\lambda_2$ and μ=μ_1+j$\omega\mu_2$, respectively [6]. Since λ is about 10^3 times larger than μ for soft tissue due to non-compressibility [6], $k_{\rm p}$ is approximated by $k_{\rm b}$. Since $k_{\rm L}$ is close to $k_{\rm s}$, $\eta \approx k_{\rm L}$ and $\eta_{\rm b} \approx k_{\rm L}$. Therefore, $f(k_{\rm L}, k_{\rm p}, k_{\rm s})$ of Eq. (1) is approximated by

$$\begin{aligned} f'(c_{\rm L}, \mu, \omega) \;=\; & 4k_{\rm L}^3\beta\cosh(k_{\rm L}h)\sinh(\beta h)) \\ & -(2k_{\rm L}^2 - k_{\rm s}^2)^2\sinh(k_{\rm L}h)\cosh(\beta h) \\ & -k_{\rm s}^4\cosh(k_{\rm L}h)\cosh(\beta h) = 0, \qquad (2) \end{aligned}$$

where $k_{\rm L}$=$\omega/c_{\rm L}(\mu,\omega)$ and $k_{\rm s}$=$\omega\sqrt{\rho_{\rm m}/\mu}$. Thus, $f'(c_{\rm L}, \mu, \omega)$ depends on both the phase velocity $c_{\rm L}(\mu,\omega)$ of the Lamb wave and the Lamé elastic constant μ=μ_1+j$\omega\mu_2$, that is, the elasticity μ_1 and the viscosity μ_2 are estimated so that the theoretical value of the phase velocity $c_{\rm L}(\mu,\omega)$ of the Lamb wave is to be close to the measured the dispersion of the phase velocity $c_{\rm phase}(\omega)$.

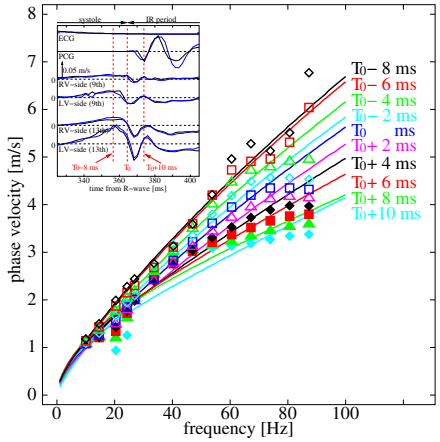

Fig. 5. Measured instantaneous phase velocity values $\{c_{\rm phase}\}$ and fitted theoretical curves $\widehat{c_{\rm L}}(\widehat{\mu}, f)$ for the frequency components from 10 Hz to 90 Hz during the period from T_0-8 ms to T_0+10 ms in left upper figure.

IV. *In Vivo* Experimental Results

For subject A, by analyzing the period from T_0-8 ms to T_0+10 ms for each frequency component from 10 Hz to 90 Hz, the instantaneous phase velocity $c_{\rm phase}(\omega)$ was obtained as in **Fig. 5**. There is large dispersion among the instantaneous phase velocities $\{c_{\rm phase}(\omega)\}$, and they rapidly decrease for all frequency components in this short period around the time of AVC (T_0).

The estimated elasticity μ_1 is about 24−30 kPa and does not change around the time of AVC. The instantaneous viscosity μ_2 of the myocardium rapidly decreases from about 400 Pa·s to 70 Pa·s. This would be due to the rapid decrease in the LV inner pressure from about 120 mmHg to several mmHg, which is caused by relaxation of the myocardium.

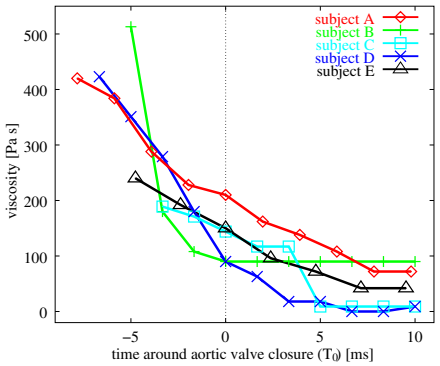

Fig. 6. Transient of the viscosity parameters $\{\mu_2\}$ measured during the period from T_0-8 ms to T_0+10 ms for five healthy young male subjects.

For the other four subjects, B−E, the same measurement and analysis were applied, and similar transient characteristics of the viscosity were obtained as shown in **Fig. 6**.

Using the estimated Lamé constant $\widehat{\mu}$, the phase velocity $\widehat{c_{\rm L}}(\widehat{\mu}, f)$ is obtained. The results are shown by the solid lines in **Fig. 5** for each time t. The estimates $\{\widehat{c_{\rm L}}(\widehat{\mu}, f)\}$ well fit the measured dispersion characteristics $c_{\rm phase}(f)$.

V. Phase Velocity for Each Layer of IVS

For patients with HCM, parallel alignment of muscle cells becomes irregular (myocardial disarray). In literature, the anisotropy of the speed of sound and the elastic properties have been measured in *in vitro* experiments. In the actual heart wall, along the radial axis (the thickness direction) of the LV, the myocardial fiber orientation changes gradually. In this study, for subject D, the IVS was divided into 5 layers along the ultrasonic beams and for each layer the phase velocity of the Lamb wave was determined as shown in **Fig. 7**. The phase velocity decreased during the short period just after the AVC (T_0). The phase velocity in the middle layer was lower than those in the LV-side and RV-side of the heart wall. This result will corresponds to the change in myocardial fiber orientations.

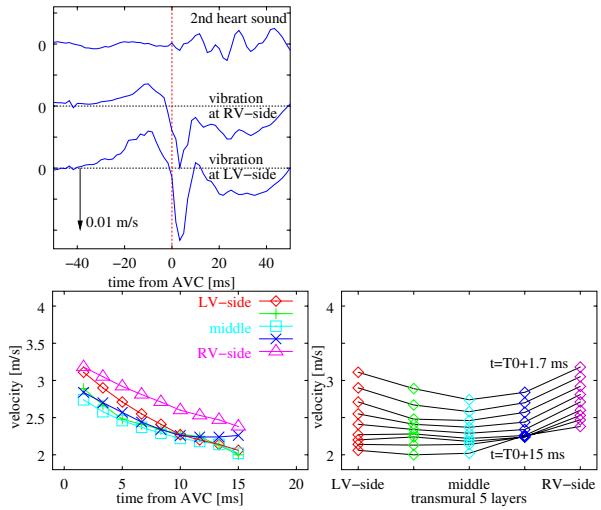

Fig. 7. The phase velocity of each of 5 layers set in the IVS for healthy subject D.

VI. Discussion

The elastic values and viscosity values obtained in the present study are compared with those reported for the myocardium and soft tissues in the literature using audio or lower frequency components up to 10 kHz as shown in **Fig. 8**. Except for those of the present study, all data were measured in *in vitro* experiments. Roughly speaking, the elasticity is large for very low frequency less than 10 Hz and for frequency higher than 1 MHz. In [12], the experimental results for pig kidney showed that the elasticity increases with frequency in the frequency range from 0.01 Hz to 20 Hz. The viscosity data are well fitted to μ_2=626.7$\times f^{-0.722}$ [Pa·s], which shows that the viscosity decreases with the increase in frequency f. By considering the frequency dependency and the freshness of the specimen in **Fig. 8**, the elasticity and viscosity measured in the present study are close to those measured for the same frequency range in the literature.

VII. Conclusions

We measured rapid and minute vibrations simultaneously at multiple points in the IVS. Clear propagation of the pulsive wave along the IVS was recognized. From the dispersion

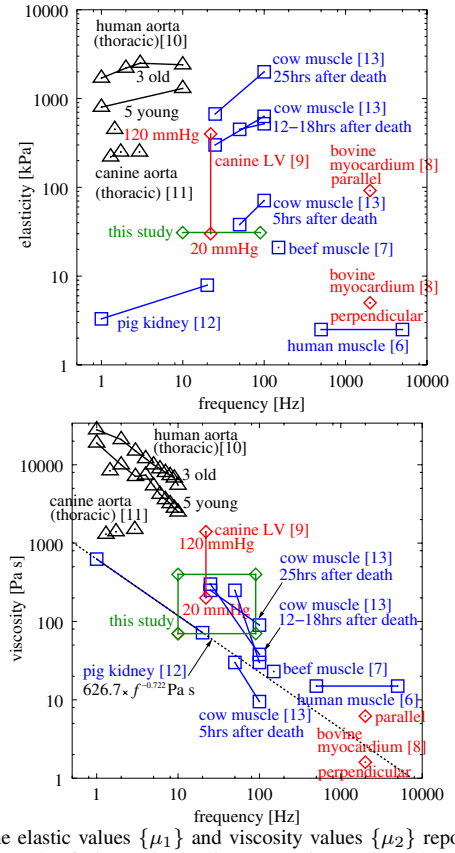

Fig. 8. The elastic values $\{\mu_1\}$ and viscosity values $\{\mu_2\}$ reported for the myocardium and soft tissues in the literature using audio or lower frequency components up to 10 kHz.

of the phase velocities, the myocardial viscoelasticity was determined noninvasively for the first time. This method offers potential for *in vivo* imaging of the spatial distribution of the passive mechanical properties of the myocardium and its rapid change during the IR period, which would enable direct assessment of diastolic properties based on myocardial relaxation in heart failure.

The author is grateful to Prof. Emeritus Motonao Tanaka and Prof. Yoshiro Koiwa of Tohoku University.

References

[1] G. R. Sutherland, *et al.*, *J. Am. Soc. Echocardiogr.*, vol. 17, pp. 788-802, 2004.
[2] H. Kanai, *et al.*, *IEEE Trans. UFFC.*, vol. 43, pp. 791-810, 1996.
[3] H. Kanai and Y. Koiwa, *Ultrasound Med. Biol.*, vol. 27, pp. 481-498, 2001.
[4] H. Kanai, *2004 IEEE International Ultrason. Sympo. Proc.*, pp. 482-485, 2004.
[5] T. Kundo, *Ultrasonic Nondestructive Evaluation*, New York: CRC Press, 2003.
[6] H. L. Oestreicher, *J. Acoust. Soc. Am.*, vol. 23, pp. 707-714, 1951.
[7] S. Catheline, *et al.*, *J. Acoust. Soc. Am.*, vol. 105, pp. 2941-2950, 1999.
[8] P.-K. Choi, *et al.*, *The IEICE Trans.*, vol. J84-A, pp. 1439-1443, 2001.(in Japanese)
[9] G. H. Templeton and L. R. Nardizzi, *J. Appl. Physiol.*, vol. 36, pp. 123-127, 1974.
[10] B. M. Learoyd, M. G. Taylor, *Circ. Res.*, vol. 18, pp. 278-292, 1966.
[11] B. S. Gow and M. G. Taylor, *Circ. Res.* vol. 23, pp. 111-122, 1968.
[12] S. Nasseri, *et al.*, *Rheol. Acta*, vol. 41, pp. 180-192, 2002.
[13] E. R. Fitzgerald, *et al.*, *J. Acoust. Soc. Am.*, vol. 29, pp. 61-64, 1957.